23

Metal Stabilization Mechanisms in Recycling Metal-Bearing Waste Materials for Ceramic Products

Kaimin Shih and Xiuqing Lu
Department of Civil Engineering, University of Hong Kong Hong Kong SAR China

1. Introduction

Ceramic materials are essential to a wide range of marketable products, and are of diverse compositions and characteristics. The effective thermal reaction capable of achieving mineral phase transformation is a unique and beneficial opportunity to convert many types of metals into more environment-ally friendly forms. This characteristic may be of particular value to the sustainable development in the 21st century, when more and more attention is focused on environment protection. It is well known that discharge of hazardous metals into natural environments, such as water bodies and soils, is detrimental to human health and the ecosystem. For example, nickel and copper enter the human body via food and water consumption. For human beings, continued inhalation of nickel and its compounds can cause lung cancer, while acute nickel exposure can lead to a variety of clinical symptoms, such as gastrointestinal disturbances, visual disturbance, headache and giddiness, and so on. For animals, prolonged exposure to nickel can lead to adverse effects on haematological parameters, decreased body weights and cancer and, therefore, nickel compounds are often treated as carcinogenic substances (Gang & Zhuang, 2007). Similarly, high accumulation of copper in human body is detrimental to liver and may even cause deadly cirrhosis (European Copper Institute [ECI], 2008). A large amount of waste containing hazardous metals is generated in a wide variety of industries, such as mining and ore processing, metallurgy, chemical industry, alloys industry, paint industry, glass industry, pulp and paper mills, leather tanning, textile dyeing and printing, chemical fertilizer, chloro-alkali industry, petroleum refining and coal burning (Agarwal, 2009). Some municipal solid wastes also contain hazardous metals, such as electrical and electronic equipments waste, barriers, paints and so on. In 2000, the total amount of hazardous waste in China was as much as 830 million tons (State Environmental Protection Administration of China, 2001). It's reported that hazardous waste of up to 963 million tons was generated in 2004, which was 116% of that in 2000 (State Environmental Protection Administration of China, 2005). In the United States, it has been reported that about 40% of hazardous wastes contain heavy metals (Hirschhorn & Oldenburg, 1991).

Traditional wastewater treatment methods use physiochemical processes, such as precipitation, coagulation, reduction, ion exchange, and membrane processes such as ultrafiltration, electrodialysis, and reverse osmosis to remove the pollutants (Park et al.,

2005). However, such physiochemical processes can also result in large quantities of hazardous metals getting into the resulting sludge which requires further treatment into a type of solid waste. Ashes and sludge containing these hazardous metals are usually more difficult to be treated because of their persistence for both biological and chemical degradation, compared to organic wastes and many other chemical pollutants. Moreover, metal concentration increases after degradation of organic materials. Therefore, sludge or its post-incineration ashes generated from municipal and industrial wastewater treatment processes have also become an increasingly serious problem for many regions in the world.

The use of low-cost sorbents has been investigated as an effective way to remove hazardous metals from water. Natural materials or waste products from certain industries having high capacity for accommodating hazardous metals can be employed at lower costs. These sorbents may include bark, chitosan, xanthate, zeolite, clay, peat moss, seaweed and dead biomass (Bailey et al., 1999). The mechanism of these cost-effective methods is to form a net negative charge to hold the hazardous cations; the large surface area of these materials also contributes to the absorption. Nevertheless, such a mechanism is without chemical bonding and may not be stable enough to resist acidic attacks under certain natural environments. In addition, the spent sorbents may also be subject to the corresponding treatment and disposal.

Although a number of processing strategies have the capability to recover metals from solids, metals commonly contained in sludge or spent sorbents are still difficult to be recycled. One common strategy currently adopted to dispose hazardous metal sludge or ashes of incinerated spent sorbent is landfill. However, due to the non-degradable property of metals, leachates of landfills may contain higher levels of hazardous metals, and thus may cause potential pollution to the surrounding land and groundwater resources (Alejandro, 2007a, 2007b; Bilgili 2006). Therefore, the U.S. Environmental Protection Agency (EPA) has proposed the Land Disposal Restriction (LDR) program to set up more strict standards for land disposal of hazardous sludge. LDR regulation requires that hazardous wastes must meet protective treatment standards before disposal in landfill. It also demands these wastes be stored in secure landfills with no hydraulic contact, restricted access, and continuous monitoring (Shih, 2005; Knecht, 2001). Since land resources have become more limited while the quantity of wastes is continuously increasing, the cost of landfill process will inevitably be higher in the future. Therefore, strong attention has been focused on the more economical and environmentally friendly alternatives to dispose hazardous-metal bearing sludge.

Portland cement is a type of hydraulic cement commonly used around the world. It is produced by pulverizing clinkers consisting essentially of hydraulic calcium silicates and contains one or more forms of calcium sulfate. Portland cement is usually added as a binder to stabilize/solidify heavy metals (Douglas & Brandstetr, 1990). After a short hydration period, the slurry mixture of heavy-metal wastes and Portland cement can be solidified. As a result, wastes are solidified in the mixture (Hou et al., 2006). With further mechanistic study of cement solidification, the main stabilization processes are found to be precipitation, chemisorption and encapsulation (Gougar et al., 1996; Andac & Glasser, 1999; Yousuf et al., 1995), rather than incorporating them into crystalline matrices, and such immobilization mechanisms may be reversible in many conditions. Experiments have showed that Portland cement binders may not be able to prevent heavy metals leaching in acidic environments (Cheeseman et al., 1993; Yousuf et al., 1995). For example, under the attack of dissolved CO_2 in natural environments, leaching of solidified metals may be highly affected by the decreased pH value (Lange et al., 1997; Andac & Glasser, 1999; Stegemann et al., 2000).

However, if hazardous metal ions are incorporated into crystalline matrices of minerals, they may usually achieve higher stability. Glass-bonded zeolite has been developed as a high-level waste form for nuclear waste generated during pyroprocessing of spent fuel from the Integral Fast Reactor (IFR) (Lewis et al., 1994; Sun et al., 1999). Treated radioactive wastes with remarkable leaching resistivity were then stored in geological repositories. Such a stabilization/solidification method for hazardous metals has been proven to be very promising for radioactive wastes. Nevertheless, if geological repositories or landfill facilities are still needed for disposal of treated wastes, such methods will still pose a serious problem because of paucity of land. If an environmental strategy is able to manage a closed-loop material flow by reusing and recycling hazardous waste to produce marketable products, it can help preserve the environment on a sustainable basis. Besides being a resolution of environmental problems, such a strategy can also create new resources and facilitate production of products. Addition of materials regenerated from waste may impact quality of products adversely but financial returns from sale of the new products can at least compensate the processing cost (André, 2010). Such a strategy will be a major step toward more sustainable development in the 21st century. It has drawn high interest from many researchers. Experiments have successfully demonstrated that hazardous metal waste can be sintered into ceramic raw materials to produce new ceramics with excellent leaching resistance (Wiebusch & Seyfried, 1997; Chen & Lin, 2009; Vieira et al., 1999).

Ceramic materials of diverse compositions and characteristics often have a crystalline or partially crystalline structure. They are brittle, hard and strong in compression and weak in shearing and tension, and are able to withstand chemical attack in an acidic or caustic environment. An effective thermal reaction capable of achieving mineral phase transformation could be a beneficial opportunity to convert many types of metals into their more environmentally friendly forms. The beneficial use of waste materials for ceramic sintering processes is a sustainable way of reducing the waste problem and it provides the new raw materials for the industry at the same time. Sintering clays with metal-bearing sludge has been employed to treat waste materials and to generate new bricks and tiles (Wiebusch & Seyfried, 1997; Reinosa et al., 2010; Zhang et al., 2007). By aiming at industrial application, such ceramic products were sometimes proven to be with even better mechanical performance than traditional bricks and tiles, in terms of properties such as hardness, transverse rupture strength, abrasion and erosion (Vieira et al., 1999). Hazardous metals immobilized in the new construction ceramic products also show excellent resistance against the leaching test (Zhang et al., 2007). To create a successful waste-to-resource strategy, the mechanism and efficiency of removing or deactivating pollutants in the waste need to be clearly identified and quantitatively evaluated for reliable control of product safety and quality. In the mechanistic study of thermal reaction, simulation of hazardous metals by their oxides may further illustrate the phase transformation process and provide the basic incorporation efficiency information.

Recent works involving mechanistic investigation of stabilizing of nickel and copper waste solids in alumina and iron-rich ceramics have had major breakthroughs in understanding of incorporation efficiencies and product leaching behavior (Hu et al. 2010; Shih, 2005, 2006a, 2006b, 2007; Tang et al., 2010). Such findings are crucial for the development of beneficial usage of metal bearing waste materials and for safely blending them into ceramic raw materials for manufacturing marketable products. Therefore, this chapter systematically introduces current developments in identified stabilization mechanisms, incorporation efficiencies, and observed metal leaching properties of product phases. Finally, the derived

technical information is organized to suggest the feasibility of this waste-to-resource strategy.

2. Metal stabilization mechanisms

To facilitate the observation of metal stabilization mechanisms, the corresponding metal oxides were selected to simulate the solidification process and to simplify the system. Nickel and copper were selected as the target metals, and their oxide forms, NiO and CuO, were chosen to simulate metal-bearing sludge for sintering, as most of them exist as oxide forms at high temperatures. Kaolinite and alumina, both commonly found in ceramic raw materials, were used to incorporate nickel and copper. In addition, although iron is not a major element in ceramic raw materials, it often exists in ceramic raw materials as an impurity. Therefore, hematite, a common iron oxide phase, was also selected as a precursor for the incorporation test. As one of the most important processing parameters, sintering temperature was controlled in the range of 800 °C to 1480 °C to be corresponding to the temperature range currently being used in the ceramic industry. For a wider fit with industrial production processes, a short sintering time scheme of 3 h to 6 h was adopted.

2.1 Qualitative analysis by X-Ray Diffraction (XRD)

After its discovery by Wilhelm Conrad Röntgen, the X-ray technique has been applied to detect broken bones and metal cracks because of its penetrating ability (Lin, 1983). In 1919, Hull A. W. found that a crystalline substance gave a unique X-ray diffraction (XRD) pattern, just as a fingerprint. Since then, the XRD technique analysis has become one of the most powerful techniques for identifying crystalline materials and investigating crystal structures (Mittemeijer and Scardi, 2003).

When an X-ray beam impinges a crystalline sample whose atoms or molecules are arranged regularly, the scattered waves interact with each other and form new strengthening or weakening waves, also known as diffraction. The intensity and position of waves (called line profile or peak) in diffraction patterns are different. They can be used to identify the size and shape of the unit cell of the crystalline sample when comparing them with the standard patterns which come from a certain authorized database. In this study, Powder Diffraction Files (PDF) database of International Centre for Diffraction Data (ICDD) was selected as the standard patterns database. Considering that incorporating hazardous metals into ceramic materials leads to phase transformation, XRD technique was employed to investigate the reaction pathways and explore the metal stabilization mechanisms.

2.2 Ceramic raw materials

Kaolin, chiefly composed of kaolinite ($Al_2O_3 \cdot 2SiO_2 \cdot 2H_2O$), is considered to be one of the richest forms of clay in nature. After being preheated at 700°C for 12 hours, major elemental compositions of the kaolin material used in this study are expressed in their corresponding oxide forms (Fig. 1). Percentages of Si and Al elements expressed in SiO_2 and Al_2O_3 forms are 45.1% and 38.6%, respectively, in the sample, similar to theoretical mass percentages (46.5% and 38.6%) derived from its chemical formula. The XRD pattern of kaolin powder also shows kaolinite as the dominant phase, when matching with the Powder Diffraction Files (PDF) database of International Centre for Diffraction Data (ICDD) (Fig. 2 (a)).

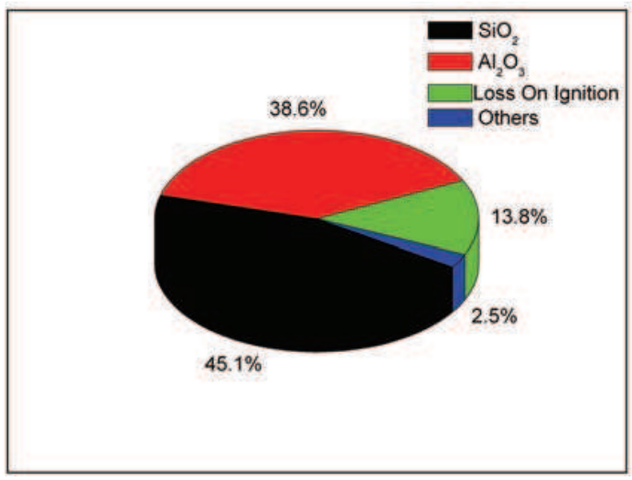

Fig. 1. Major elements (by weight, percentage) expressed in the forms of metal oxides for kaolin powder.

When heated, kaolinite transfers to the other Si-Al phases known as the kaolinite-mullite series. To investigate roles of different phases in incorporation of hazardous metals, phases within the kaolinite-mullite series were produced by heating kaolin raw materials at different temperatures. After heating at 600°C, kaolinite lost its physically bound water and was converted into amorphous substances (Fig. 2 (b)), which is believed to be metakaolin ($2Al_2O_3 \cdot 4SiO_2$), according to previous studies (Brindley and Nakahira, 1959). When the temperature was at or above 980°C, metakaolin changes into a poorly crystallized phase which may be one of the following reactions:

$$2Al_2O_3 \cdot 4SiO_2 \text{ (metakaolin)} \rightarrow 0.375Si_8[Al_{10.67}\square_{5.33}]O_{32} + SiO_2 \quad (1)$$

$$2Al_2O_3 \cdot 4SiO_2 \text{ (metakaolin)} \rightarrow 0.188Al_8[Al_{13.33}\square_{2.66}]O_{32} + 4SiO_2 \quad (2)$$

Where □ represents vacancy and the defect spinel $Al_8[Al_{13.33}\square_{2.66}]O_{32}$, is generally believed to be γ-Al_2O_3. However, metakaolin at 980°C is difficult to be identified by X-ray diffraction technology, due to its poorly crystallized nature. After sintering kaolin at 990°C for 3 hours (Fig. 2 (c)), the weak but still detectable peaks at around 2θ =37°, 46° and 67° are similar to characteristic peaks of γ-Al_2O_3 (Zhou and Snyde, 1990). Transformation is followed by mullite ($3Al_2O_3 \cdot 2SiO_2$) and cristobalite (SiO_2) formation at 1200°C (Fig. 2 (d)). When heating temperature reached 1480°C, the intensive peak of cristobalite at around 2θ=24° indicated nearly all amorphous silica had been crystallized to cristobalite (Fig. 2 (e)).

Since aluminium is suspected to be one of the major metals to react with nickel and copper, alumina (Al_2O_3) was also used as a raw material to simulate the processes of metal incorporation. Alumina has several polymorphs, including crystalline corundum (α-Al_2O_3) and metastable phases with defect crystal structures, such as γ-, η- and θ-alumina (Wolverton and Hass, 2000; Zhou and Snyder, 1990). γ-Al_2O_3, an important technological material with high surface area, can be converted from boehimite at 975°C and transformed into corundum by further calcination at above 1200°C (Shih and Leckie, 2007). Both γ-Al_2O_3 and α-Al_2O_3 were used as aluminium-rich precursors to immobilize hazardous nickel and copper metals in this study. As Fig. 3 shows, after heating HiQ®-7223 alumina powder

(boehmite, AlOOH, ICCD PDF#72-0359) at 650°C for 6h and 1500°C for 3 hours, γ- and α-Al_2O_3 were formed.

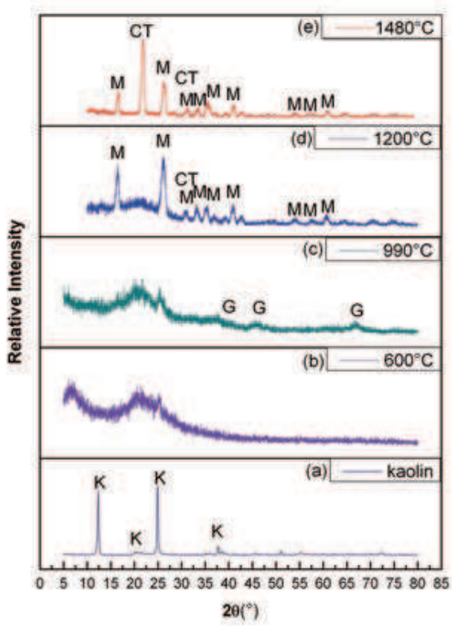

Fig. 2. X-ray diffraction (XRD) patterns of (a) USP grade acid-washed kaolin powder, and after being heated at (b) 600 °C/3 h, (c) 990 °C/3 h, (d) 1200 °C/3 h and (e) 1480 °C/3 h. "K" represents the peak positions of the referenced kaolinite (ICDD PDF#78-1996), "G" for γ-Al_2O_3, "CT" for cristobalite (SiO_2, ICDD PDF#76-0938) and "M" for mullite(ICDD PDF#79-1445).

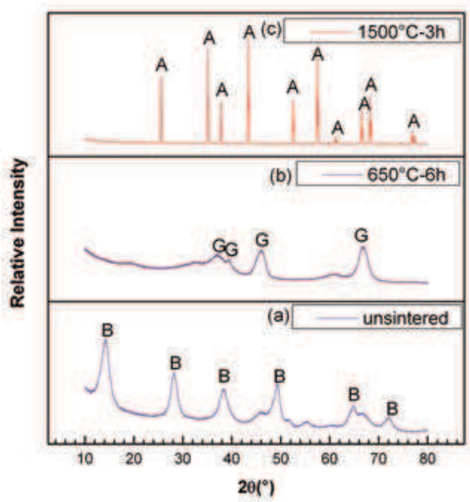

Fig. 3. XRD patterns of (a) HiQ®-7223 alumina powder, and sintered HiQ®-7223 alumina powder at (b) 650 °C/6 h, and (c) 1500 °C/3 h. "B" represents for beohmite (AlOOH, ICCD PDF#72-0359), "G" for γ-Al_2O_3, and "A" for corundum (α-Al_2O_3, ICCD PDF#76-0144)

2.3 Spinel formation

When sintering the mixture of nickel oxide and kaolinite, nickel spinel ($NiAl_2O_4$) was discovered from XRD patterns (Fig. 4(d)). In that experiment, an extended 6 hour sintering was designed to further facilitate the attainment of near equilibrium and observation of product phases. Molar ratio of Ni and Al was fixed at 1:2, corresponding with the molecular formula of nickel aluminate spinel. At 900°C, the sintered kaolinite was transferred into amorphous metakaolin (Fig. 4(a)), and no spinel was detected in the calcined mixture of kaolinite and nickel oxide (Fig. 4(c)). However, when sintering temperature was increased to 990°C, a poorly crystalline phase appeared, as shown in Fig. 4(b), at 2θ around 37°, 46° and 67°. Regardless of the true composition of this defect spinel phase, positions of its diffraction peaks were similar to those of γ-Al_2O_3 (Zhou and Snyde, 1990). When NiO was mixed in the same kaolinite precursor, formation of new nickel aluminate spinel phase in the product could be observed due to occurrence of diffraction peaks at different 2θ positions (Fig. 4(d)).

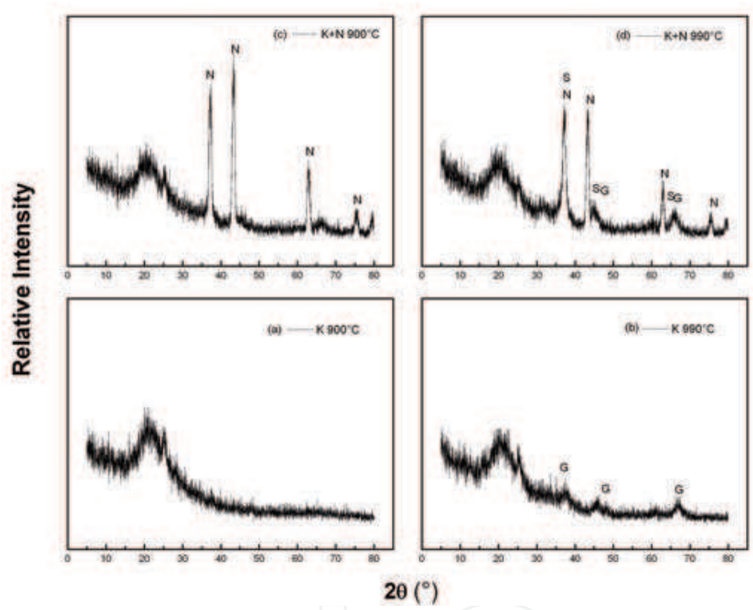

Fig. 4. XRD patterns of the 6 h sintered (a) kaolinite (K) at 900°C, (b) kaolinite 990°C, (c) kaolinite with NiO (N) at 990°C, and (d) kaolinite with NiO at 900°C. "G" represents for the peaks of γ-Al_2O_3, "N" for NiO (ICDD PDF#78-0429), and "S" for $NiAl_2O_4$ (ICDD PDF#78-0552).

Considering the defect spinel structure derived from kaolinite, as shown in Eqs. (1) and (2), the possible mechanism for the formation of nickel aluminate spinel at this sintering temperature may be:

$$NiO + \gamma\text{-}Al_2O_3 \rightarrow NiAl_2O_4 \quad (3)$$

$$5.33NiO + Si_8Al_{10.67}O_{32} \rightarrow 5.33NiAl_2O_4 + 8SiO_2 \quad (4)$$

However, due to very poor crystalline nature of these defect spinel structures, the XRD technique was not able to identify which reaction, i.e. Eq. (3) or Eq. (4), is the mechanism of forming nickel aluminate spinel in the 990°C and 3 h sintered kaolinite + NiO sample. The

formation of $NiAl_2O_4$ from sintering the NiO and Al_2O_3 mixture has been widely studied, and a phase diagram of NiO-Al_2O_3 system at temperatures above 1350°C has been presented (Philips et al., 1963). However, very few literatures have referred to reactions at temperatures lower than 1350°C. To further confirm the possible formation mechanism of $NiAl_2O_4$, γ-Al_2O_3 was selected as a precursor to react with NiO at 990°C under 6 h sintering. The XRD result (Fig. 5) not only confirms the possible reaction of Eq. (3) at the lower (< 1350 °C) temperature, but also helps indicate the potential formation mechanism of $NiAl_2O_4$ on sintering kaolinite + NiO at 990°C.

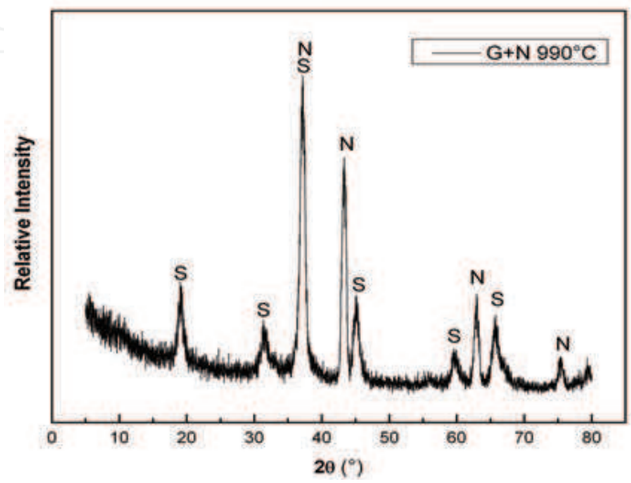

Fig. 5. XRD pattern of sintering the mixture of NiO (N) and γ-Al_2O_3 (G) at 990°C for 6 hours. "N" stands for NiO (ICDD PDF#78-0429), and "S" represents for $NiAl_2O_4$ (ICDD PDF#78-0552).

Although the presence of $NiAl_2O_4$ could be detected at 990°C on sintering NiO and kaolinite, NiO still showed strong XRD peaks in the result (Fig. 4). Therefore, higher temperatures, such as 1250°C and 1450°C, may be needed to further facilitate the mass transfer process. XRD patterns obtained from products of sintering kaolinite + NiO at 1250°C and 1450°C for 3 hours (Fig. 6(a) and Fig. 6(b)) reveal that spinel is a primary product phase, together with the crystalline cristobalite (SiO_2). The major diffraction peak of cristobalite (2θ=21.94°) at 1250°C sintered samples was weaker than the most intensive peak of $NiAl_2O_4$ (2θ=37.01°), but it turned to be stronger at 1450°C. At 1000°C, mullite starts to form with excess amorphous silica, and the silica crystallizes into cristobalite at a higher temperature. The $NiAl_2O_4$ is more likely to be formed from mullite at high temperatures due to the following reactions:

$$3[2Al_2O_3 \cdot 4SiO_2(\text{metakaolin})] \rightarrow 2[3Al_2O_3 \cdot 2SiO_2(\text{mullite})] + 8SiO_2(\text{cristobalite}) \quad (5)$$

$$3NiO + 3Al_2O_3 \cdot 2SiO_2(\text{mullite}) \rightarrow 3NiAl_2O_4 + 2SiO_2(\text{cristobalite}) \quad (6)$$

Eq. (6) was further confirmed by sintering the mixture of mullite, cristobalite and nickel oxide with a fixed molar ratio of Ni : Al : Si = 1 : 2 : 2, at 1250°C for 3 hours. The XRD patterns of the product are provided in Fig. 6(a), which shows that mullite together with nickel oxide could produce crystalline $NiAl_2O_4$, while cristobalite did not appear to have reacted with nickel oxide.

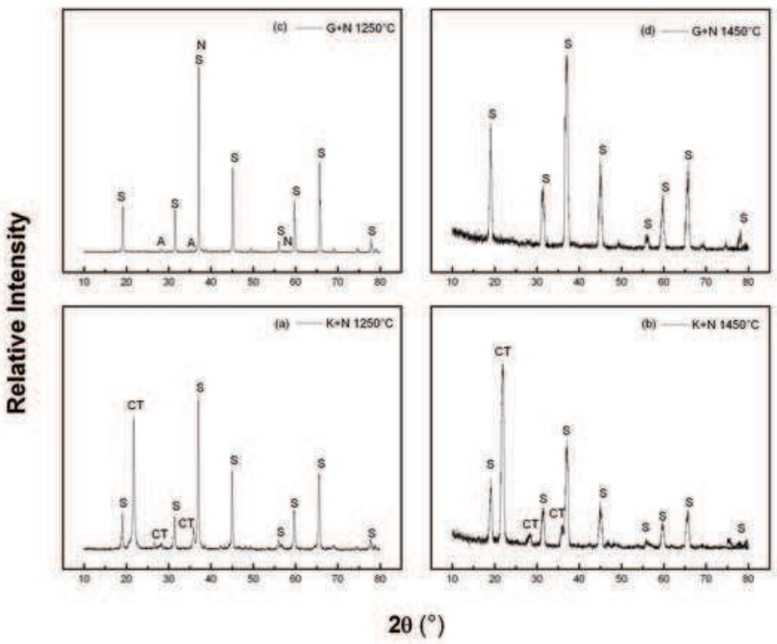

Fig. 6. XRD patterns of 3 h sintered products of (a) kaolinite (K) + NiO at 1250°C, (b) kaolinite + NiO at 1450°C, (c) γ-Al_2O_3 (G) + NiO at 1250°C, and (c) γ-Al_2O_3 (G) + NiO at 1450°C. "N" is for NiO (ICDD PDF#78-0429), "A" for corundum (α-Al2O3, ICDD PDF#83-2080), "S" for $NiAl_2O_4$ (ICDD PDF#78-0552), and "CT" for cristobalite (SiO_2, ICDD PDF#76-0938).

When being sintered with γ-Al_2O_3, nickel oxide disappeared in the system of 1450°C (Fig. 6(d)), while it was still slightly observable in the 1250°C system (Fig. 6(c)). Nickel aluminate spinel was the only detectable crystalline phase in 1450°C, while the residual NiO and corundum (α-Al_2O_3) existed in the 1250°C system, together with $NiAl_2O_4$. It has been reported that well-crystallized corundum (α-Al_2O_3) could be observed from calcining γ-Al_2O_3 at above 1200°C (Eq. (7); Shih and Leckie 2007). Therefore, besides the potential mechanism of Eq. (3) in the low temperature range, nickel incorporation may be proceeded with by two possible steps at higher temperatures:

$$\gamma\text{-}Al_2O_3 \rightarrow \alpha\text{-}Al_2O_3 \quad (7)$$

$$NiO + \alpha\text{-}Al_2O_3 \rightarrow NiAl_2O_4 \quad (8)$$

Feasibility of reaction represented in Eq. (8) was confirmed by the calcined product of α-Al_2O_3 and NiO with molar ratio of Ni : Al = 1:2 at 1250°C for 3 hours. The XRD pattern in Fig. 7(b) reveals that $NiAl_2O_4$ was the only phase in the product without detectable residual reactants. By comparing the XRD pattern of Fig. 6(c) to that of Fig. 7(b), it appears that at 1250°C, the spinel formation rate from sintering α-Al_2O_3 + NiO is higher than that from sintering NiO + γ-Al_2O_3.

When the aluminum-rich precursors were replaced by iron-rich precursors, similar spinel formation reaction was observed, as shown in Fig. 7(c). Nonoverlaid peaks, i.e. at 2θ around 18.4°, 30.2°, and 35.6°, clearly indicated the formation of nickel ferrite spinel ($NiFe_2O_4$, trevorite) from the sintered iron oxide and nickel oxide mixture under 1250°C for 3 h.

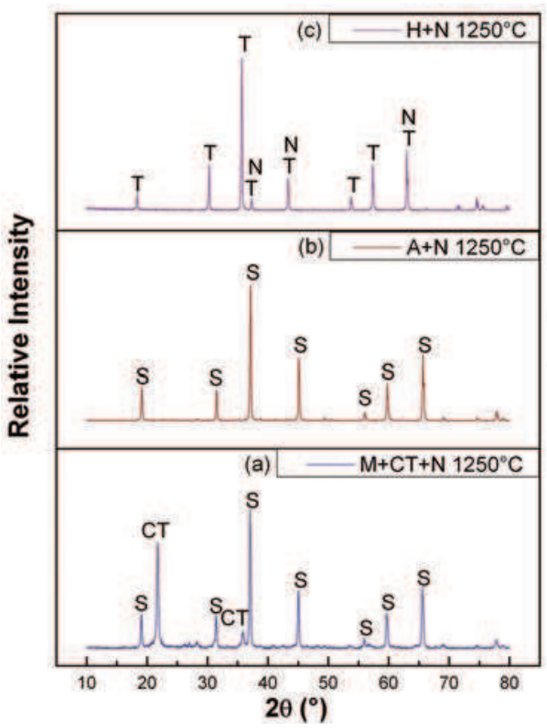

Fig. 7. XRD patterns of sintering (a) mullite(M) + cristobalite(CT) + NiO(N), (b) α-Al_2O_3(A) + NiO(N), (c) hematite(H) + NiO(N) at 1250°C for 3 hours. "S" stands for nickel aluminate spinel ($NiAl_2O_4$, ICDD PDF#78-0552), "CT" for cristobalite (SiO_2, ICDD PDF#76-0938), and "T" for nickel ferrite spinel ($NiFe_2O_4$, trevorite, ICDD PDF#86-2267).

Therefore, the thermal reaction between NiO and Fe_2O_3 as provided in the following equation could be a potential pathway for producing $NiFe_2O_4$:

$$NiO + Fe_2O_3\,(\text{hematite}) \rightarrow NiFe_2O_4 \tag{9}$$

When being sintered with kaolinite at 1000°C for 3 hours, substantial copper was incorporated into the copper aluminate spinel ($CuAl_2O_4$) structure, which clearly acted as a host to accommodate the hazardous copper in high temperature environments (Fig. 8(a)). The diffraction pattern of sintering the γ-Al_2O_3 + CuO system at 1000°C for 3 h indicates a large portion of copper in copper oxide has been successfully converted into spinel (Fig. 8(b)). The results indicate a feasible way to tackle the copper waste problem by sintering it with kaolinite or other aluminium-rich precursors for marketable ceramic products.

3. Incorporation efficiency

From the qualitative information provided in the previous section, metal incorporation is found to play an important role in determining composition of the final products. High temperature usually increases the reaction rate and leads to high incorporation efficiency. Sintering time is a parameter highly related to productivity of industrial process and energy cost. Therefore, the quantitative relationship between temperature and incorporation efficiency is of great importance for the design of reliable methods to effectively incorporate the metals into ceramic products. Metal incorporation efficiency at the temperature range

from 600°C - 1480°C was investigated by a 3 h short sintering scheme to reveal such a relation in the metal stabilization process.

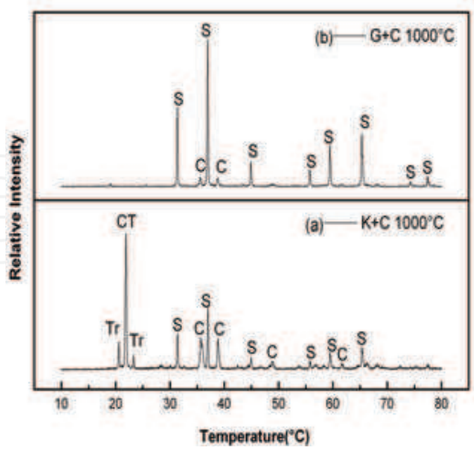

Fig. 8. XRD patterns of (a) kaolinite(K) + CuO(C) mixture sintered at 1000°C for 3 h, and (b) γ-Al_2O_3(G) + CuO mixture sintered at 1000°C for 3 h. "S" represents for $CuAl_2O_4$ (ICDD PDF#76-2295), "C" for CuO (ICDD PDF#48-1548), "CT" for cristobalite (SiO_2, ICDD PDF#76-0935), and "Tr" for tridymite (SiO_2, ICDD PDF#88-1535).

3.1 Quantitative XRD technique

Quantitative analysis of XRD data usually involves determination of the amounts in specific phases in a specimen, by modelling the observed XRD patterns. In this study, metal incorporation efficiencies for different precursors and temperatures were estimated by quantitative XRD analysis, using the Whole Pattern Fitting (WPF) strategy to model XRD patterns. The WPF was carried out by using the Pawley method integrated into a XRD data processing software, JADE (Material Data, Inc). Phase quantification by WPF was executed by matching the observed XRD patterns with the PDF database of ICDD. In this study, the weight percentage of each crystalline phase was generated together with the weighted (R) and expected (E) reliability values to indicate the quality of fitting for each refinement. Weighted and expected reliability values are calculated by the following equations:

$$R(\%) = 100 \times \sqrt{\frac{\sum[w(i) \times (I(o,i) - I(c,i))^2]}{\sum[w(i) \times (I(o,i)) - I(b,i))^2]}} \tag{10}$$

$$E(\%) = 100 \times \sqrt{\frac{(N - P)}{\sum I(o,i)}} \tag{11}$$

where I (o,i) and I (c,i) represent the observed intensity and calculated intensity of a fitted data point (i), respectively; I (b,i) is the background intensity of point (i); w (i) is the weight of the data point, as w(i)=1/I(o,i); N is the number of fitted data points and P is the number of refined parameters. The ratio of R/E, which is equal to 1 in an ideal model, stands for "goodness of fit", but due to the existence of background intensity, it's often greater than one.

3.2 Transformation ratio

To define metal incorporation efficiency, an index of transformation ratio (TR) was designed, as the following equation:

$$TR(\%) = \frac{\frac{wt\% \text{ of } MX_2O_4}{\text{MW of } MX_2O_4}}{\left(\frac{wt\% \text{ of } MX_2O_4}{\text{MW of } MX_2O_4} + \frac{wt\% \text{ of MO}}{\text{MW of MO}}\right)} \quad (12)$$

where M stands for metal ions (Ni or Cu in this study); X is Al or Fe; and MW means molecular weight. When TR = 0, no metal incorporates into the precursor, while all metal incorporate into precursors when TR = 100%.

Although the large amount of amorphous silica at temperature below 1150°C had made the quantitative analysis difficult, efficiencies of Ni incorporation by kaolinite and mullite precursors are shown in Fig. 9 (a), which demonstrates that both precursors can achieve a high Ni incorporation efficiency (more than 90%) at temperatures above 1160°C. In Fig. 9 (a), TR of kaolinite + NiO system is around 10% higher than that of mullite + cristobalite + NiO system when sintering at 1150°C for 3 hours.

Fig. 9 (b) shows nickel aluminate spinel generated from sintering the two NiO + Al_2O_3 mixtures at over 600°C. In terms of nickel incorporation efficiency, more than 90% of nickel in the α-Al_2O_3 precursor was transformed into $NiAl_2O_4$ structure at over 1250°C. It is also interesting to find a crossover point of these two alumina systems at around 1150°C in Fig. 9 (b), which demonstrates that reaction of NiO and γ-Al_2O_3 dominated at lower temperatures while corundum (α-Al_2O_3) precursor facilitated nickel incorporation at higher temperatures. Assigning k_1, k_2 and k_3 to stand for reaction rates of γ-Al_2O_3 reacting with NiO (Eq. 3), γ-Al_2O_3 transforming to corundum (Eq. 7), and NiO incorporating into corundum (Eq. 8), respectively, the higher free energy of γ-Al_2O_3 leads its reaction with nickel oxide to being more favourable energetically ($k_1 > k_3$) and then further obtains its higher incorporation efficiency at temperature below 1150°C. When temperature was increased, k_2 exceeded k_1, so reactions of both alumina precursors are likely identical with the case of having α-Al_2O_3 reacting with NiO.

$$NiO + \gamma\text{-}Al_2O_3 \xrightarrow{k_1} NiAl_2O_4 \quad (3)$$

$$\gamma\text{-}Al_2O_3 \xrightarrow{k_2} \alpha\text{-}Al_2O_3 \quad (7)$$

$$NiO + \alpha\text{-}Al_2O_3 \xrightarrow{k_3} NiAl_2O_4 \quad (8)$$

At high temperatures, silica content may be a potential flux to further facilitate mass transfer during the reaction, and thus the higher TR may occur in the system using kaolinite or mullite as precursors, compared to results of Al_2O_3 + NiO systems shown in Figs. 9 (a) and 9 (b). Compared to the interaction between nickel oxide and kaolinite under 900°C for 6 hours (Fig. 4 (c)), the transformation level of Ni in the NiO + hematite system was already much higher (~90%) even with sintering at 900°C for only 3 hours (Fig. 7). Furthermore, from TR curves of NiO + kaolinite and NiO + hematite (Fig. 9 (b) and Fig. 9 (c)), it appears that the ferrite spinel can be formed at a lower temperature range. This indicates that nickel bearing sludge may first react with iron impurities, before initiating reactions with kaolinite-based ceramic precursors during immobilization of hazardous nickel waste in ceramics.

For the case of copper incorporation, a low temperature range (650°C – 1000°C) was designed to investigate incorporation efficiency. As shown in Fig. 10, incorporation efficiency of CuO + γ-Al_2O_3 system is generally higher than that of CuO + kaolinite system.

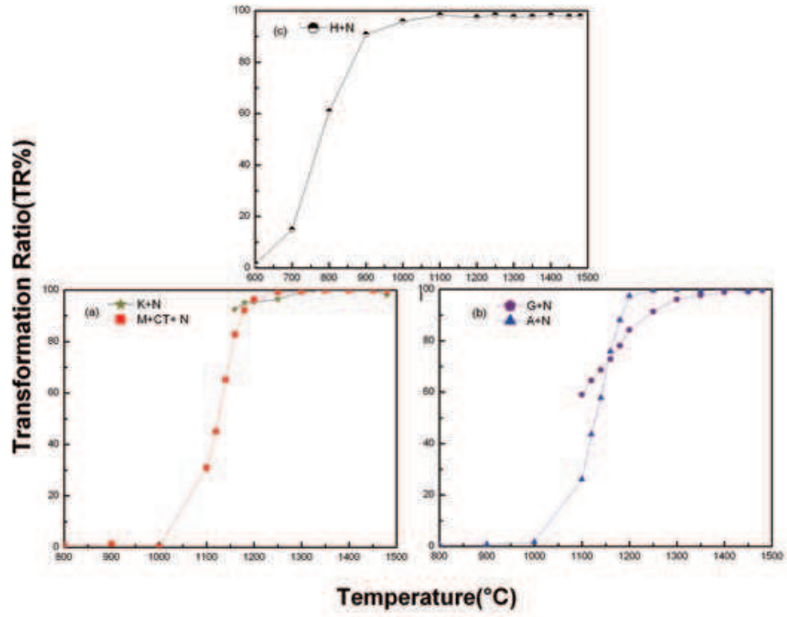

Fig. 9. Nickel incorporation efficiency when sintering NiO with different precursors for 3 hours: (a) kaolinite(K) from 1160°C to 1480°C and mullite(M) + cristobalite(CT) from 800°C to 1480°C; (b) γ-Al_2O_3(G) from 1100°C to 1480°C and α-Al_2O_3(G) from 800°C to 1480°C; and (c) hematite(H) from 600°C to 1480°C.

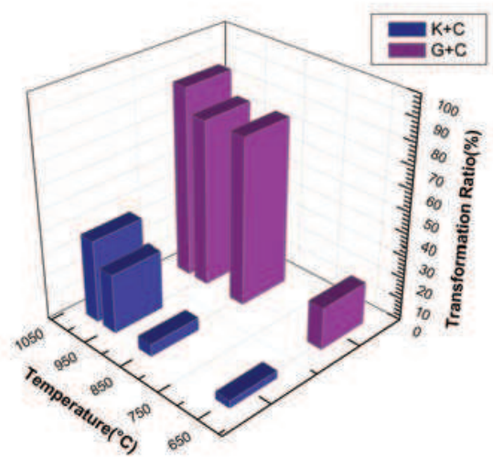

Fig. 10. Efficiency of copper incorporation by kaolinite and γ-Al_2O_3 precursors with 3 h sintering under 650°C, 850°C, 950°C and 1000°C. "K" represents kaolinite, "G" denotes γ-Al_2O_3, and "C" CuO.

The highest copper incorporation efficiency observed in CuO + γ-Al_2O_3 system was nearly 90% in TR, when the sample was sintered at 1000°C for 3 hours. Incorporation efficiency of CuO + kaolinite system was also found to increase with increase of sintering temperature, although incorporation efficiency was lower than that of the CuO + γ-Al_2O_3 system. A maximum of 33% copper incorporation was observed when sintering CuO with kaolinite precursor at 1000°C for 3 hours, and this result may still suggest the important contribution of kaolinite in stabilizing copper in copper-bearing sludge under ceramic sintering processes.

4. Metal leachability and leaching behavior

Since the major purpose of incorporating hazardous metal waste into ceramic products is to immobilize the waste and prevent contamination of the environment, leachability and leaching behavior of metals from the new product phases are of great importance to determine whether such products are more environmentally benign than their original forms.

4.1 Design of leaching experiment

The "Toxicity Characteristic Leaching Procedure (TCLP)" is a method designed by U.S. EPA to determine mobility of both organic and inorganic analytes present in liquid, solid and multiphasic wastes at a laboratory level. For solid phase, extraction fluid # 1 (pH = 4.88 ± 0.05 acetic + NaOH solution) or extraction fluid # 2 (pH = 2.88 ± 0.05 acetic solution) is used for the test, with the amount of extraction fluid equal to 20 times the weight of the solid phase (Environment Protection Agency [EPA], 1992). In this study, 10 ml of the more acidic # 2 extraction solution was applied to leach a 0.5 g solid sample. To further test the spinel leachability over a longer period and under harsher conditions, standard TCLP test was modified by grinding the samples into powders, to reach a larger surface area, as well as for prolonging leaching time to more than 20 days.

To further transform reactants into the designated spinels, the same oxide raw materials as were used in the previous spinel formation sections were mixed in molar ratio of 0.5 for Ni/Al, Ni/Fe, and Cu/Al systems to generate single phase $NiAl_2O_4$, $NiFe_2O_4$ and $CuAl_2O_4$ samples, respectively. Considering more than 98% TR under sintering at 1480°C for 3 hours (Fig. 9), extended treatment for 48 hours at 1480°C was used to convert NiO + γ-Al_2O_3 and NiO + hematite into $NiAl_2O_4$ and $NiFe_2O_4$, respectively. To form the single phase $CuAl_2O_4$ sample, CuO + γ-Al_2O_3 was under 990°C thermal treatment for 20 days. All products were ground into powders for XRD analysis to confirm the signal phase results in the products, as well as for BET analysis to evaluate their surface areas. The 0.5 g powder sample and 10 mL of # 2 extraction solution were filled into each leaching vial, which was then rotated end-over-end during the leaching time. At the designated sampling time, the collected leachate was filtered and diluted to measure ion concentrations by inductively coupled plasma atomic emission spectroscopy (ICP-AES). Four replications of samples collected at each time point were performed to reduce random errors.

4.2 Metal leaching results

After thermal processing at 1480°C for 48 hours, the NiO(N) + γ-Al_2O_3(G) mixture formed $NiAl_2O_4$; the NiO + kaolinite(K) mixture was converted into $NiAl_2O_4$ + cristbolite (SiO_2); and

the NiO + hematite (H) mixture resulted in $NiFe_2O_4$. Changes of pH values in sample leachates are shown in Fig. 11. In the first few days, pH values of NiO (a) and $NiAl_2O_4$ (b) leachates increased rapidly, while pH of $NiFe_2O_4$ (c) leachate and sintered NiO + kaolinite (d) had only slight increases. After the first few days, pH values of NiO leachate gradually increased, but pH of leachates from $NiAl_2O_4$, sintered NiO + kaolinite, and $NiFe_2O_4$ samples maintained more stable levels till the end of leaching period (more than 25 days). As a higher pH in leachate stands for fewer protons in a solution, a larger change of pH value indicates that more protons have been consumed. A potential reason for the change of pH is the exchange of metal ions in solids with protons in the solution, which leads to decrease of proton concentrations in the leachate. Therefore, such change of pH value may imply higher long term acid resistance of sintered products, and it also illustrates that the leaching time of standard TCLP (18 h) may not be able to reflect long term leachability of the low soluble materials.

Because nickel leachability in spinel determines the quality of immobilization of hazardous metals in ceramics, concentrations of nickel in leachates were measured. From BET analysis, surface areas of different sample powders were determined to be 3.6 ± 0.5 m^2/g for NiO, 1.1 ± 0.1 m^2/g for $NiAl_2O_4$, 0.73 ± 0.12 m^2/g for sintered NiO + kaolinite ($NiAl_2O_4$ + cristobalite), and 1.7 ± 0.2 m^2/g for $NiFe_2O_4$. In addition to surface area, nickel content in each nickel containing compound, i.e. NiO, $NiAl_2O_4$, $NiAl_2O_4$ + cristobalite, and $NiFe_2O_4$, should also be normalized for comparison.

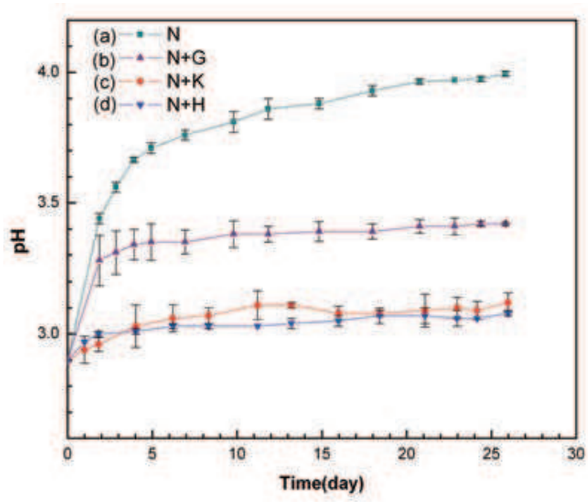

Fig. 11. The pH values of leachates from (a) NiO(N), and the 1480°C/48 h sintered (b) NiO + γ-Al_2O_3(G), (c) NiO + kaolinite(K), and (d) NiO + hematite(H). The product of (b) is $NiAl_2O_4$; of (c) is $NiAl_2O_4$ + cristobalite(SiO_2); and of (d) is trevorite($NiFe_2O_4$). The 0.5 g solid sample powder was leached by 10 ml # 2 extraction solution (acetic acid, pH = 2.9) for a period ranging from 0.75 day to 26 days. The mixture of powder sample and extraction solution was rotated end-over-end during the leaching period.

In Fig. 12, surface-area and metal-content normalized nickel concentrations in leachates illustrate the result of comparing the intrinsic leachability of different nickel bearing phases. Nickel in $NiAl_2O_4$ + cristobalite sample was found to be more invulnerable to acid attack, which may be due to encapsulation of cristobalite matrix for nickel aluminate spinel.

$NiFe_2O_4$ showed a higher leachability than NiO in the first two days, but the trend changed to a much slower process than that of NiO in the prolonged leaching period. Potential reason for the higher leachability of $NiFe_2O_4$ at the initial stage was likely due to incomplete formation of $NiFe_2O_4$ or acid attack on its weaker grain boundary. Although leaching curves of $NiAl_2O_4$ and $NiFe_2O_4$ were quite similar, $NiFe_2O_4$ shows a much smaller change of pH value than $NiAl_2O_4$ in Fig. 11. If the leaching mechanisms of these two spinels are the same, changes of their pH values should be similar. Therefore, further investigation was conducted to compare the results of the other ions leached out of these two solids.

For congruent dissolution, molar ratio of Ni/Al and Ni/Fe in leachates should be equal to 0.5 for both $NiAl_2O_4$ and $NiFe_2O_4$ phases. Fig. 13 (a) summarizes the Ni/Al ratio in the leachate and the result of Ni/Al ~ 0.5 confirmed the behavior of congruent dissolution for $NiAl_2O_4$. However, similar comparison found that Ni/Fe ratio in leachate of $NiFe_2O_4$ was much higher than 0.5, as shown in Fig. 13 (b). One possible explanation for the high Ni/Fe ratios is incongruent dissolution of Ni and Fe from the $NiFe_2O_4$ structure, which is different from the case of leaching $NiAl_2O_4$. Another possible explanation is that after the congruent dissolution of Ni and Fe from $NiAl_2O_4$, the Fe re-precipitated on the surface of particles.

At pH of around 3.0, the dissolved Fe may exist in the forms of Fe^{3+}, $FeOH^{2+}$, $Fe(OH)_2^+$ and $Fe(OH)_4^-$. From a pC-pH diagram of $Fe(OH)_{3\bullet Am}$, the total dissolved Fe concentration approximates to 0.88 ppm, which is considerably close to Fe concentrations detected in this study (0.5 ppm - 1.0 ppm). Therefore, regardless of the leaching mechanism of $NiFe_2O_4$, composition of its leachate was mainly controlled by reprecipitation of amorphous $Fe(OH)_3$ solid.

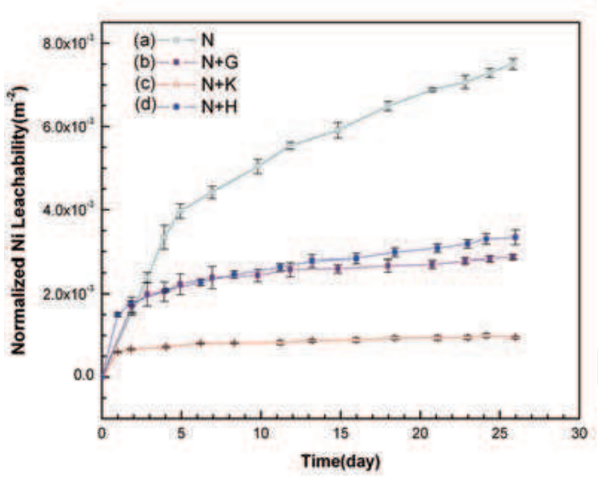

Fig. 12. Normalized Ni concentrations in leachates of (a) NiO(N), and the 1480°C/48 h sintered (b) NiO + γ-Al_2O_3(G), (c) NiO + kaolinite(K), and (d) NiO + hematite(H). The product of (b) is $NiAl_2O_4$; of (c) is $NiAl_2O_4$ + cristobalite(SiO_2); and of (d) is trevorite ($NiFe_2O_4$). The 0.5 g powder samples were leached by 10 ml # 2 extraction solution (acetic acid, pH = 2.9) over a period of time ranging from 0.75 day to 26 days. The mixture of sample and solution was rotated end-over-end during the leaching period. The Ni concentrations in leachates were normalized by the powder sample surface areas and nickel contents.

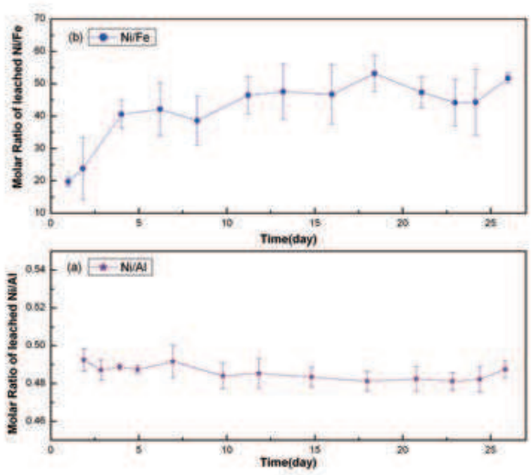

Fig. 13. Molar ratios of leached [Ni]/[Al] in (a) $NiAl_2O_4$ leachates, and [Ni]/[Fe] in (b) $NiFe_2O_4$ leachates. The leaching test was conducted using 10 mL TCLP # 2 extraction solution (acetic acid, pH = 2.9) to leach 0.5 g powder for 0.75 day ~ 26 days.

In the 22 days leaching period for copper-bearing phases, similar acid resisting capacity was found for copper aluminate spinel ($CuAl_2O_4$). As Fig. 14 shows, pH values of CuO leachates increased rapidly in the first two days, and then stabilized at around 4.9. However, pH values of $CuAl_2O_4$ leachates (b) were maintained at around 3.1, which indicates that much fewer protons had been consumed from the leaching solution, compared to CuO leachates during the leaching period. The normalized Cu leachability also clearly indicates the higher acid resistance of copper aluminate spinel (Fig. 15).

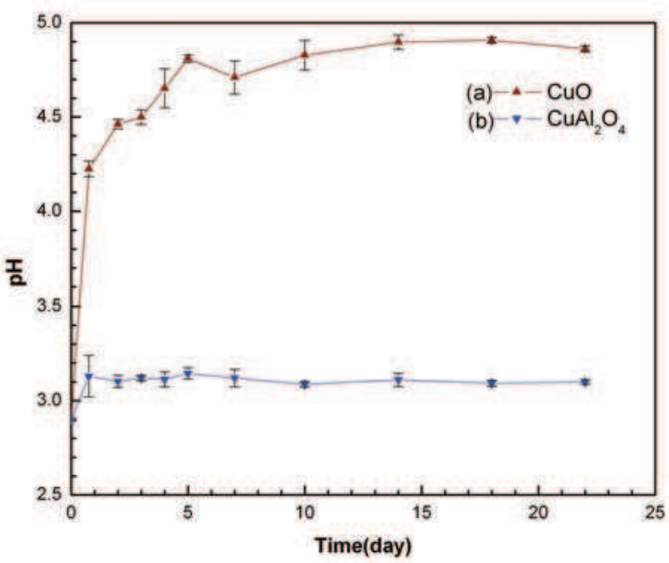

Fig. 14. The change of pH values of (a) CuO, and (b) $CuAl_2O_4$. The $CuAl_2O_4$ was prepared by sintering CuO+ γ-Al_2O_3 at 990°C for 20 days. The 0.5 g powder sample was added into 10 ml TCLP No. 2 extraction solution (pH ~ 2.9) and the vial was rotated end-over-end for 0.75 day~22 days.

Very little copper was leached from the $CuAl_2O_4$ solid sample; more copper was dissolved from CuO solid after normalization of sample surface area and copper content. The considerable difference between $CuAl_2O_4$ and CuO not only implies the superior acid resistivity of $CuAl_2O_4$, but also indicates that the waste containing copper oxide needs further stabilization before disposal.

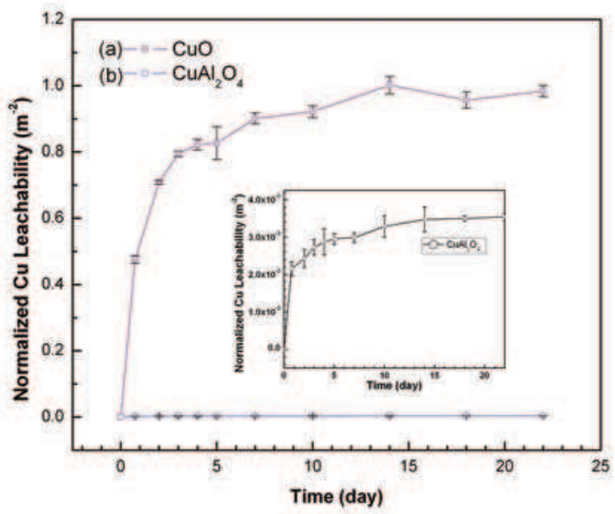

Fig. 15. Normalized Cu leachablity of (a) CuO; and (b) $CuAl_2O_4$. The $CuAl_2O_4$ was prepared by sintering CuO + γ-Al_2O_3 at 990°C for 20 days. Each leaching vial was filled with 10 ml TCLP extraction solution # 2 (acetic acid with a pH = 2.9) and 0.5 g powder sample. These vials were then rotated for 0.75 day and 22 days. Copper concentrations in leachates were normalized by different surface areas and Cu contents in the solid samples.

5. Conclusions

To investigate mechanisms of immobilization of hazardous waste metals by ceramic materials, nickel oxide and copper oxide were used to simulate the metal bearing sludge and sintered with a variety of ceramic precursors. The incorporation mechanisms together with reaction efficiencies were also identified to facilitate optimization of metal incorporation. To confirm the environmentally benign property of product phases, a modified leaching test was carried out to evaluate the amounts of leached hazardous metals. The changes of pH values were observed to reflect the degree of metal leaching, and the measured metal concentrations in leachates were normalized by solid surface area and metal content to reflect the intrinsic properties of the product phases. Overall, the current progress of recycling metal bearing waste for ceramic products can be organized as follows.

For results of incorporating nickel:

- Nickel oxide can react with kaolinite, mullite, γ-Al_2O_3 and α-Al_2O_3 under thermal conditions to form $NiAl_2O_4$; and with Fe_2O_3 to produce $NiFe_2O_4$.
- NiO can react with the defect spinel structure derived from kaolinite precursor at low temperature to form spinel, and it can also react with mullite to form $NiAl_2O_4$ at higher temperature.

- When reacting with aluminium-rich and iron-rich precursors, more than 90% of nickel oxide can be converted into spinel phase at temperatures above 1250°C.
- When sintering NiO with kaolinite and mullite precursors at high temperatures, SiO_2 content may act as a flux to facilitate the mass transfer.
- The formation temperature of $NiFe_2O_4$ is about 200°C lower than that of $NiAl_2O_4$, and, therefore, nickel may first react with Fe_2O_3 to form ferrite in ceramic products.
- Spinel-containing products show remarkable resistance to protonic attacks by pH 2.9 acetic acid solution.
- Leaching of $NiFe_2O_4$ may be accompanied by reprecipitation of amorphous $Fe(OH)_3$ from the leachate.

For the results of incorporating copper:

- Calcination of CuO with γ-Al_2O_3 or kaolinite precursor could produce copper aluminate spinel ($CuAl_2O_4$).
- When the sintering temperature is lower than 1000°C, transformation ratio of CuO + γ-Al_2O_3 system will be much higher than that of CuO + kaolinite system.
- The normalized copper leachability of CuO was found much higher than that of $CuAl_2O_4$ and this indicates that the CuO is quite vulnerable to acid attack, while $CuAl_2O_4$ shows much stronger intrinsic acid resistance.

As significant amount of nickel oxide was still found as the residual in alumina-rich systems when sintering temperature was below 1140°C, one needs to be cautious in attempts to incorporate nickel-bearing waste at such low temperatures in ceramic products, such as manufacturing of bricks or low-grade porous construction ceramics. However, similar work has revealed that copper bearing waste may be further transformed into copper spinel at temperatures below 1000°C, considering the 87% copper transformation ratio when sintering CuO and γ-Al_2O_3. Therefore, the current mechanistic development of incorporating hazardous metals into ceramic products is of great importance as it provides key information on applicability of incorporating different types of metals into marketable ceramic products as a waste-to-resource strategy.

6. References

Agarwal, S. K. (2009). *Heavy metal pollution,* A P H Publishing Corporation, Delhi, India.

Alejandro, S. & Jacint, N. (2007). Bioaccumulation of Metals and Effects of Landfill Pollution in Small Mammals. Part I. The Greater White-toothed Shrew, Crocidura Russula. *Chemosphere,* Vol. 68, pp. 703-711.

Alejandro, S. & Jacint, N. (2007). Bioaccumulation of Metals and Effects of a Landfill in Small Mammals. Part II. The Wood Mouse, Apodemu Sylvaticus. *Chemosphere,* Vol. 70, pp. 101-109.

Andac, M. & Glasser, F. P. (1999). Long-term Leaching Mechanisms of Portland Cement-Stabilized Municipal Solid Waste Fly Ash in Carbonated Water. *Cement and Concrete Research,* Vol. 29, No. 2, pp. 179-186.

André, Z. (2010). Ceramic Products from Waste. In: *Ceramic Materials*, InTech, ISBN 978-953-307-145-9, Vienna, Austria.

Bailey, S. E.; Olin, R. J.; Brickea, M. & Adrian D. A. (1999). A Review of Potentially Low-Cost Sorbents for Heavy Metals. *Water Research*, Vol. 33, No. 11, pp. 2469-2479.

Bilgili, M. S.; Demir, A.; Ince, M. & Ozkaya, B. (2006). Metal Concentrations of Simulated Aerobic and Anaerobic Pilot Scale Landfill Reactors. *Journal of Hazardous Materials,* Vol. 145, pp. 186-194.

Brindley, G. W. & Nakahira, M. (1959). Aolinite-Mullite Reaction Series: Ⅱ, Metakaolin. *Journal of the American Ceramic Society*, Vol. 42, No. 7, pp. 14-318.

Cheeseman, C. R.; Butcher, E. J.; Sollars, C. J. & Perry, R. (1993). Heavy Metal Leaching from Hydroxide, Sulphide and Silicate Stabilized/Solidified Wastes. *Waste Management*, Vol. 13, No. 8, pp. 545-552.

Chen, L. & Lin, D. F. (2009). Applications of Sewage Sludge Ash and Nano-SiO_2 to Manufacture Tile as Construction Material. *Construction and Building Materials*, Vol. 23, No. 11, pp. 3312-3320.

Douglas, E. & Brandstetr, J. (1990). A Preliminary Study on the Alkali Activation of Ground Granulated Blast-Furnace Slag, *Cement and Concrete Research*, Vol. 20, No. 5, pp. 746-756, ISSN: 00088846.

Environment Protection Agent (1992). Toxic Characteristic Leaching Procedure, (accessed in February 2011), available from: http://www.epa.gov/osw/hazard/testmethods/sw846/pdfs/1311.pdf

European Copper Institute (2008). European Union Risk Assessment Report, In: European Chemical Agent, 10.01.2011, (accessed in February 2011), available from: http://echa.europa.eu/chem_data/transit_measures/vrar_en.asp

Gang, B. & Zhuang, Z. (2000). Nickel Toxicology Research Progress in China. *Healthy Toxicology*, Vol. 14, No. 3, pp. 129-135.

Gougar, M. L. D.; Scheetz, B. E. & Roy, D. M. (1996). Ettingite and C-S-H Protland Cement Phases for Waste Ion Immobilization: A Review. *Waste Management*, Vol. 16, No. 4, pp. 295-330.

Hirschhorn, J. & Oldenburg, K. (1991). *Prosperity Without Pollution : the Prevention Strategy for Industry and Consumers*, Van Nostrand Reinhold, New York.

Hou, H.; He X.; Zhu, S. & Zhang, D. (2006). The Cement Solidification of Municipal Solid Waste Incineration Fly Ash. *Journal of Wuhan University of Technology*, Vol. 21, No. 4, pp. 137-140.

Hu, C. Y.; Shih, K. & Leckie J. O. (2010). Formation of Copper Aluminate Spinel and Cuprous Aluminate Delafossite to Thermally Stabilize Simulated Copper-Laden Sludge. *Journal of Hazardous Materials*, Vol. 181, pp. 399-404.

Knecht, M. A. (2001). Overview of U.S. Federal Laws and Regulations Affecting Mixed Waste Treatment. In : *Hazardous and Radioactive Waste Treatment Technologies Handbook,* CRP Press, ISBN 978-08493-9586-4.

Lange, L.; Hills C. D. & Poole, A. B. (1997). Effect of Carbonation on Properties of Blended and Non-blended Cement Solidified Waste Forms. *Journal of Hazardous Materials*, Vol. 52, No. 2-3, pp. 171-191.

Lewis, M. A.; Fischer, D. & Murphy, C. (1994). Properties of Glass-bonded Zeolite Monoliths. In: *American Ceramic Society*. Indianapolis, Indiana.

Lin, L. (1983). Principles and Application of X-ray Diffraction. *Industry Materials*, Vol. 86, pp. 100-109.

Mittemeijer, E. J. & Scardi, P. (2003). *Diffraction Analysis of the Microstructure of Materials.* ISBN: 3-540-40519-4, Springer, Verlag Berlin Heidelberg New York.

Park, D.; Lee, D. S.; Park, J. M.; Chun, H. D.; Park, S. K.; Jistuhara, I.; Miki, O. & Kato, T. (2005). Metal Recovery from Electroplating Wastewater Usign Scidophilic Iron Oxidizing Bacteria: Pilot-Scale Feasibility Test. *Ind. Eng. Cjem. Res.*, Vol. 44, pp. 1854-1859.

Philips, B.; Hutta, J. J. & Warshaw, I. (1963). Phase Equilibria in the System NiO-Al_2O_3-SiO. *Journal of the American Ceramic Society*, Vol. 46, No. 12, pp. 579-583.

Reinosa, J. J.; Silva A. C.; Rubio-Marcos, F.; Mello-Castanho, S. R. H.; Moya, J. S. & Fernandez, J. F. (2010). High Chemical Stability of Stoneware Tiles Containing Waste Metals . J*ournal of the European Ceramic Society*, Vol. 30, No. 14, pp. 2997-3004.

Shih, K. & Leckie J. O. (2007). Nickel Aluminate Spinel Formation during Sintering of Simulated Ni-Laden Sludge and Kaolinite. *Journal of the European Ceramic Society* Vol. 27, pp. 91-99.

Shih, K.; White, T. J. & Leckie J. O. (2006a). Spinel Formation for Stabilizing Simulated Ni-Laden Sludge with Aluminum-Rich Ceramic Precursors. *Environmental Science and Technology.* Vol. 40, No. 16, pp. 5077-5083.

Shih, K.; White, T. J. &Leckie J. O. (2006b). Nickel Stabilization Efficiency of Aluminate and Ferrite Spinels and Their Leaching Behavior. *Environmental Science and Technology* Vol. 40, No. 17, pp. 5520-5526.

Shih, K. (2005). Stabilization of Nickel by Aluminum- and Iron-rich Ceramic Materials: Reaction Pathways and Product Leaching Behavior. In: *Dissertation Abstracts International*, Vol. 66-08, Section B, pp. 4423-4527, ISBN: 978-054-2286-93-3.

State Environmental Protection Administration of China (2001). The State of Environment in China in 2000. *Environmental Protection*, Vol. 07.

State Environmental Protection Administration of China (2005). The State of Environment in China in 2004. *Environmental Protection*, Vol. 06.

Stegemann, J.; Roy A.; Caldwell, R. & Paul, J. S. (2000). Understanding Environmental Leachability of Electric Arc Furnace Dust. *Journal of Environmental Engineering*, Vol. 126, No. 2, pp. 112-120.

Sun, D.; Wronkiewicz, D. J. & Simpson, L. J. (1999). A Study of Alteration Phases on Glass-Bonded Zeolite and Sodalite Using the Vapor Hydration Test. *In Proceedings of the Material Research Society Symposium*, Vol. 556, pp. 189–196.

Tang, Y.; Shih, K. & Chan K. (2010). Copper Aluminate Spinel in the Stabilization and Detoxification of Simulated Copper-Laden Sludge. *Chemosphere*, Vol. 80, pp. 275-380.

Vieira, M. T.; Catarino, L.; Oliveira, M.; Sousa, J.; Torralba, J. M. & Cambronero, L. E. G. (1999). Optimization of the Sintering Process of Rawmaterial Wastes. *Journal of Materials Processing Technology*, Vol. 92-93, pp. 97–101.

Wiebusch, B. & Seyfried, C. F. (1997). Utilization of Sewage Sludge Ashes in the Brick and Tile Industry. *Water Science and Technology*, Vol. 36, No. 11, pp. 251-258.

Wolverton, C. & Hass, K. C. (2000). Phase Stability and Structure of Spinel-based Transition Aluminas. *Physical Review B*, Vol. 63 (024102), pp. 1-10.

Yousuf, M.; Mollah, A.; Vempati, R. K.; Lin, T. C. & Cocke, D. L. (1995). The Interfacial Chemistry of Solidification/Stabilization of Metals in Cement and Pozzolanic Material Systems. *Waste Management*, Vol. 15, No. 2, pp. 137-148.

Zhang, H.; Zhao, Y. & Qi, J. (2007). Study on Use of MSWI Fly Ash in Ceramic Tile. *Journal of Hazardous Materials*, Vol. 141, No. 1, pp. 106-114.

Zhou, R. S. & Snyder, R. L. (1990). Structure and Transformation Mechnaisms of the η,γ and θ Transition Alulminas. *Acta Cryst*, B47, pp. 617-630.

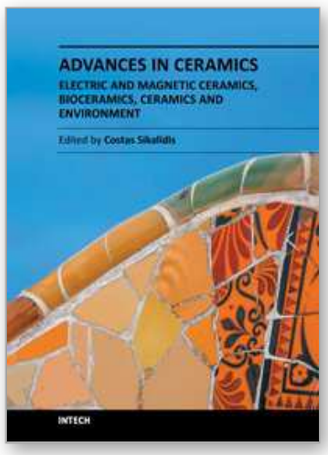

Advances in Ceramics - Electric and Magnetic Ceramics, Bioceramics, Ceramics and Environment

Edited by Prof. Costas Sikalidis

ISBN 978-953-307-350-7
Hard cover, 550 pages
Publisher InTech
Published online 06, September, 2011
Published in print edition September, 2011

The current book consists of twenty-four chapters divided into three sections. Section I includes fourteen chapters in electric and magnetic ceramics which deal with modern specific research on dielectrics and their applications, on nanodielectrics, on piezoceramics, on glass ceramics with para-, anti- or ferro-electric active phases, of varistors ceramics and magnetic ceramics. Section II includes seven chapters in bioceramics which include review information and research results/data on biocompatibility, on medical applications of alumina, zirconia, silicon nitride, ZrO2, bioglass, apatite-wollastonite glass ceramic and b-tri-calcium phosphate. Section III includes three chapters in applications of ceramics in environmental improvement and protection, in water cleaning, in metal bearing wastes stabilization and in utilization of wastes from ceramic industry in concrete and concrete products.

InTech Europe
University Campus STeP Ri
Slavka Krautzeka 83/A
51000 Rijeka, Croatia
Phone: +385 (51) 770 447
Fax: +385 (51) 686 166
www.intechopen.com

InTech China
Unit 405, Office Block, Hotel Equatorial Shanghai
No.65, Yan An Road (West), Shanghai, 200040, China
中国上海市延安西路65号上海国际贵都大饭店办公楼405单元
Phone: +86-21-62489820
Fax: +86-21-62489821

IntechOpen